

See discussions, stats, and author profiles for this publication at: <https://www.researchgate.net/publication/264042863>

Photochemistry at the Surface of Gold Nanoprisms from Surface- Enhanced Raman Scattering Blinking

ARTICLE *in* THE JOURNAL OF PHYSICAL CHEMISTRY C · JULY 2014

Impact Factor: 4.77 · DOI: 10.1021/jp5038188

READS

132

6 AUTHORS, INCLUDING:



[Younes Abid](#)

University of Sfax

78 PUBLICATIONS 512 CITATIONS

[SEE PROFILE](#)



[Adnen Mlayah](#)

Paul Sabatier University - Toulouse III

106 PUBLICATIONS 1,425 CITATIONS

[SEE PROFILE](#)



[Leila Samia Smiri](#)

University of Carthage

94 PUBLICATIONS 804 CITATIONS

[SEE PROFILE](#)

Photochemistry at the Surface of Gold Nanoprisms from Surface-Enhanced Raman Scattering Blinking

Amine Mezni,^{†,‡} Thameur Dammak,[§] Anis Fkiri,[†] Adnen Mlayah,^{*,‡} Younes Abid,[§] and Leila Samia Smiri[†]

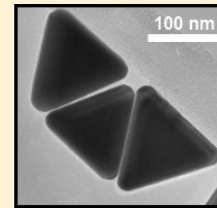
[†]Unité de recherche Synthèse et Structure de Nanomatériaux UR11ES30, Faculté des Sciences de Bizerte, Université de Carthage, 7021 Jarzouna, Tunisia

[‡]Centre d'Elaboration de Matériaux et d'Etudes Structurales, CNRS-Université de Toulouse, 29 Rue Jeanne Marvig, 31055 Toulouse, France

[§]Laboratoire de Physique Appliquée, Faculté des Sciences, Université de Sfax, BP 802, 3018 Sfax, Tunisia

S Supporting Information

ABSTRACT: In this work, we investigate the optical properties of triangular gold nanoprisms synthesized following a one-pot chemical process and using triethylene glycol (TREG) and polyvinylpyrrolidone (PVP) as solvent and capping agents. The nanoprisms sustain a strong localized surface plasmon resonance (LSPR) which is exploited in surface-enhanced Raman scattering (SERS) by the PVP and TREG molecules present at the nanoparticle surface. The work is focused on the temporal fluctuations of the SERS signal. The assignment of the observed Raman features is based on density functional theory calculations, performed for various interaction states between the PVP or the TREG molecules and the gold surface, in a simple model system. The SERS blinking is analyzed quantitatively using the autocorrelation of spectrally selected temporal SERS traces. We also use SERS covariance maps in order to investigate the cross-correlation between the relevant Raman features. We show that the fluctuations of the PVP and TREG SERS signals are not random. We found that the Raman features associated with the CO stretching vibrations are fingerprints of the interaction between the organic molecules and the nanoparticle surface. In particular, we observe quasi-periodic adsorption/desorption events of the PVP molecules that reveal their dynamical interaction with the gold surface. From the SERS covariance maps, we also point out correlations between the TREG and PVP signals which we interpret as occasional exchange of the two molecular species. The dependence of the SERS blinking on the detuning between the Raman excitation and the surface plasmon resonance is also investigated. We show that the optical excitation plays an important role in the photoinduced chemical processes that occur close to the nanoparticle surface.



1. INTRODUCTION

Metallic nanoparticles are of high interest because their optical properties can be tuned throughout the visible and near-infrared electromagnetic spectrum by adjusting the nanoparticle shape, size, composition, and local dielectric environment.^{1–4} Among the variety of noble metal nanoparticles produced today, gold nanoparticles (AuNPs) with their tunable surface plasmon resonance (SPR) have attracted considerable interest due to their potential applications in catalysis, biosensing, and nanomedicine.^{5–9} The development of simple and versatile methods for the preparation of AuNPs in a size- or shape-selected and -controlled manner has been a challenging. Several published works have reported the synthesis of gold nanoparticles with various shapes using different chemical routes.^{10,11} The polyol process is a convenient, versatile, and low-cost route for the preparation of element and alloy metal nanoparticles.¹² In this process, liquid polyol or diol acts both as a solvent of the precursors and as a mild reducing reagent. Up to now, there are few reports about a simple polyol method to obtain large monodisperse triangular gold nanoparticles.

On the other hand, the collective oscillations of conduction electrons are responsible for localized surface plasmon

resonances (LSPR) and generate strong enhancement of the Raman scattering from molecules adsorbed on the nanoparticle surface. This phenomenon is widely known as surface enhanced raman scattering (SERS);^{13–16} this highly sensitive vibrational spectroscopy allows for the detection of analytes at an extremely low concentration and provides detailed information about molecular structure and dynamics in close vicinity of a nanoparticle surface.^{17,18} Huge enhancement factors of SERS (10^{10} to 10^{14}) allow researchers to sensitively measure vibrational spectra at the single molecule level^{19–21} enabling new applications in sensing²² and therapeutics.^{23,24} A characteristic feature of the SERS signal of a small number of molecules is the sudden and strong temporal fluctuations of the Raman intensities scattered at the characteristic vibrational modes.^{25,26} This so-called SERS blinking has been reported in several works and has been attributed to a variety of physical and chemical phenomena.^{27,28} SERS blinking enables the observation of the physical and chemical properties of small molecular

Received: April 18, 2014

Revised: July 8, 2014



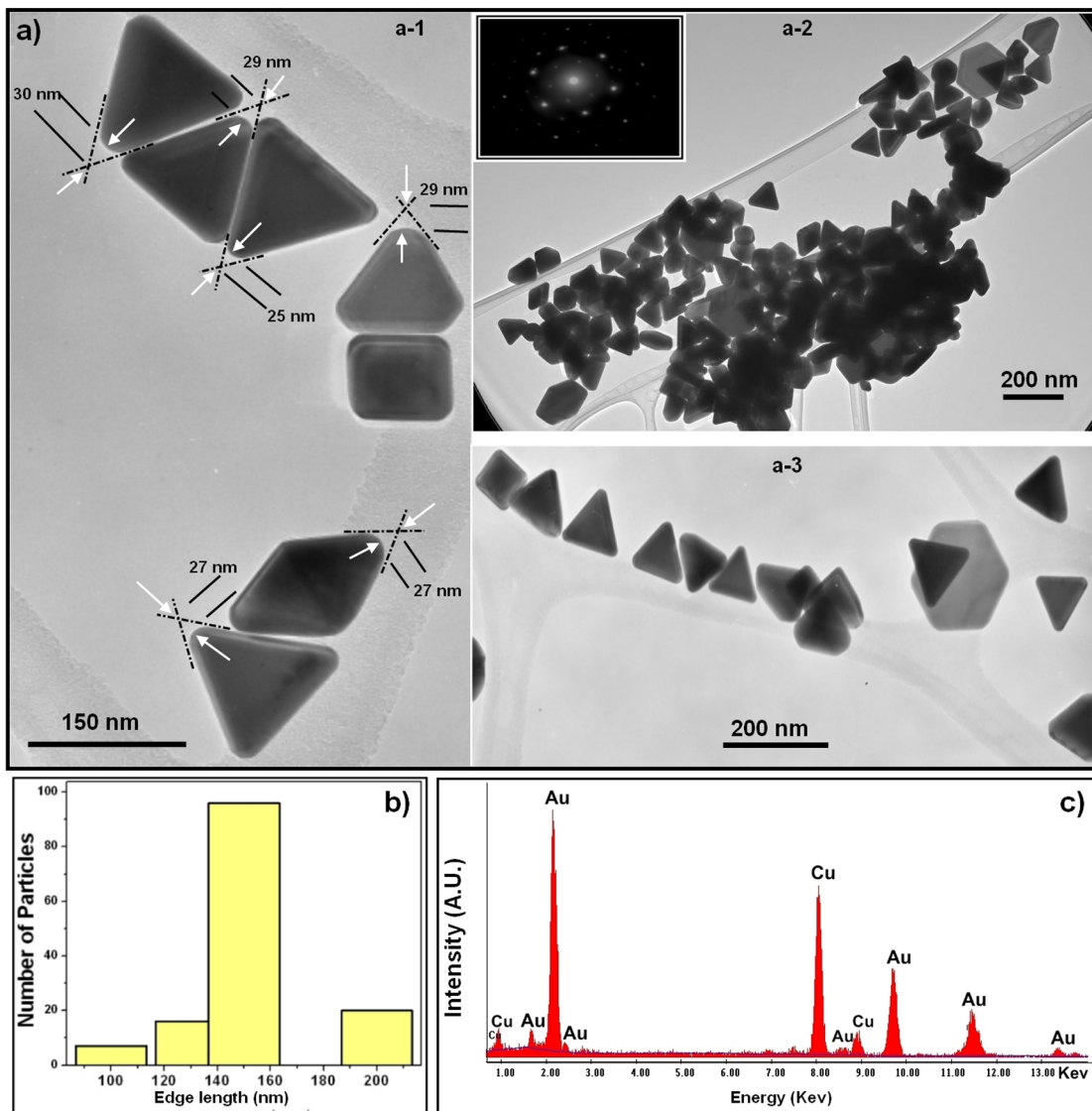


Figure 1. Transmission electron microscopy images (a1–3) of the triangular gold nanoprisms. The inset in a-2 shows a typical SAED pattern from a single nanoprism. The nanoprism face is perpendicular to the electron beam incidence. The histogram in (b) shows the distribution of the nanoprism edge length. The energy dispersive X-ray spectrum is displayed in (c). The presence of Cu in the EDX spectrum is due to the copper grid supporting the nanoparticles.

populations, which are otherwise obscured in ensemble experiments. This can contribute to the field of plasmonics to characterize the hot spots and to understand the ultrahigh enhancement observed in surface-enhanced optical spectroscopy techniques.

In this work, we exploit the LSPR properties of triangular gold nanoprisms to measure the surface-enhanced Raman scattering of the molecules adsorbed at the gold surface. The preparation of the triangular gold nanoprisms is based on a polyol synthetic strategy that makes use of triethylene glycol (TREG) as a solvent and a reducing agent in the presence of polyvinylpyrrolidone (PVP). Here, our aim is to probe the dynamical interaction between the molecular species and the nanoparticle surface using the temporal fluctuations of the SERS signal. To do so, we measure the SERS blinking spectra from several individual or small aggregate of triangular nanoprisms using confocal Raman spectroscopy. Then, on the basis of density functional theory (DFT) calculations, we assign the spectral features to molecular vibrations. In order to

identify the fingerprint of the molecule–nanoparticle surface interaction, we consider PVP and TREG molecules either free or adsorbed at the nanoparticle surface. We show that the vibrations of the CO bond in PVP and TREG is carrying the information on the molecule–nanoparticle interaction. We thus focus on the relevant spectral range and perform a quantitative analysis of the SERS spectra based on the autocorrelation traces of the Raman intensity fluctuations and their Fourier transform. We also use covariance calculations to investigate the cross-correlation between SERS signals in different spectral regions. Our results point to nonrandom fluctuations of the SERS blinking phenomenon in our investigated gold nanoprisms. They reflect the complex dynamics of photoinduced molecular adsorption/desorption events taking place at the nanoparticle surface. The paper is organized as follows: section 2.1 gives the synthesis method as well as the structural and optical characteristics of the triangular nanoprisms. The results are presented and discussed in section 3.

2. EXPERIMENTAL SECTION

2.1. Synthesis Method, Structural and Optical Characterizations. The triangular gold nanoprisms (Tr-AuNPs) were produced by a modified polyol process involving a surface regulating polymer the polyvinylpyrrolidone. Briefly, 25 mL of triethylene glycol (ACROS Organics, 98%) solution, containing 0.038 mmol of hydrogen tetrachloroaurate(III) trihydrate ($\text{HAuCl}_4 \cdot 3\text{H}_2\text{O}$) (from Sigma-Aldrich), and 0.05 molar ratio of PVP (K30 from Sigma-Aldrich) to HAuCl_4 were mixed and heated to 150 °C. The mixture was kept at this temperature for 30 min under continuous mechanical agitation. The final colloidal solution has a blue color. The product was separated by centrifugation, washed several times with ethanol/acetone (2:1), and dispersed in ethanol.

The size, shape, and composition of the synthesized nanoparticles were characterized by transmission electron microscopy (TEM) using a JEOL-JFC 1600 microscope operating at 100 keV and energy-dispersive X-ray spectrograph (EDX). Selected area electron diffraction patterns (SAED) were also acquired in order to determine the crystallographic orientation of the nanoprism facets.

Figure 1a shows a typical TEM image of the synthesized nanoparticles. The majority of the nanoparticles are equilateral triangular prisms with an average edge length of 150 nm as obtained from the histogram in Figure 1b. Hexagonal and elongated nanoparticles are also present. The nanoprisms are snipped; the snips are in the range 25–29 nm. Energy dispersive spectrum (EDX) spectroscopy confirms that the nanoprisms consist of only gold (Figure 1c). The inset in Figure 1a presents an SAED pattern obtained with the electron beam incidence perpendicular to the face of a single nanoprism. The hexagonal symmetrical spots of the SAED pattern reveal that the nanoprism is a monocrystal with a {111} oriented face.

The PVP/ HAuCl_4 molar ratio plays a critical role in the formation of gold nanoprisms. Indeed, because of the selective adsorption of PVP molecules on {111} oriented planes, the latter have a minimal growth rate compared to {110} and {100} planes.^{29,30} On the other hand, we suggest that the TREG molecules are also adsorbed on the {111} oriented planes and thus contribute to slow down their growth, which explains the formation of gold nanoprisms with a small PVP/ HAuCl_4 molar ratio $R = 0.05$. Indeed, the TREG is acting not only as a solvent but also as a capping/stabilizing agent which allows triangular nanoprisms to grow with a minimum amount of surfactant.³¹

The optical absorbance spectrum of the colloidal solution was recorded using a PerkinElmer Lambda 11 UV/vis setup. An extinction band with a maximum intensity around 700 nm and half width at half-maximum of approximately 300 nm is clearly visible (Figure 2). The plasmonic response of metal nanoprisms, to optical excitation, has been investigated in several published works.³² It is well-known that a metal nanoprism supports dipolar and quadrupolar surface plasmons with resonance wavelengths that depend on the nanoprism edge length, thickness and snip.³³ The TEM images do not give access to the nanoprism thickness. Therefore, in order to fully characterize the nanoprisms and determine their average thickness, we have calculated the optical response of a single nanoprism using the discrete dipole approximation (DDA) method^{34,35} and compared the results to the measured extinction spectrum. Assuming a fixed edge length of 150 nm (from TEM data Figure 1b), we have changed the thickness of the nanoprism and also considered the effect of the nanoprism

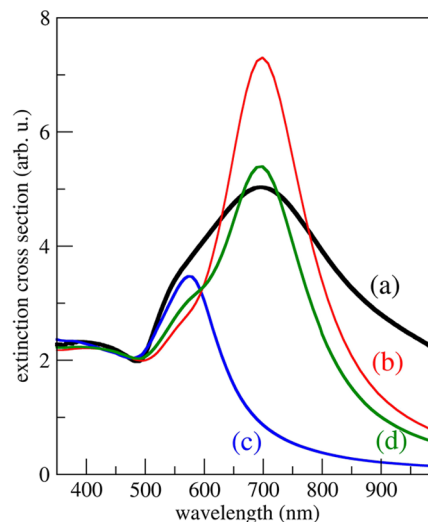


Figure 2. Measured extinction spectrum of the colloidal solution containing the triangular nanoprisms (a, black). The solvent is ethanol. The simulated extinction spectra of a single nanoprism with 150 nm edge length, 50 nm thickness, and 27.5 nm snip are shown for incident polarizations parallel (b, red) and perpendicular (c, blue) to the nanoprism face. The spectrum averaged over 50 orientations of the polarization is also shown (d, green).

snip, as the latter is responsible for a strong blue shift of the surface plasmon resonance.³⁶ As shown in Figure 2, a good agreement between the resonance wavelengths and lineshapes of the calculated and measured optical extinction spectra is obtained for an average nanoprism thickness of 50 nm and with a snip of 27.5 nm (average snip value from TEM data in Figure 1a). The calculated extinction spectrum is averaged over 50 orientations of the incident polarizations in order to allow for excitation of the planar dipolar and quadrupolar surface plasmon modes³⁷ and also of the transverse mode which is excited with an incident polarization perpendicular to the nanoprism face. This mode gives rise to a resonance around 575 nm which is clearly visible in the measured extinction spectrum as a shoulder on the short wavelength side of the main dipolar resonance. The orientation averaged spectrum reproduces quite well the experimental spectral line shape including the intensity dip around 500 nm. The fluctuations in nanoprism edge length, thickness, and snip could account for the broadening of the surface plasmon resonances. However, above 800 nm, the experimental extinction is noticeably larger than the simulated, certainly because of the contribution of nanoparticles with different shapes (rod-like, hexagonal, large spheres...) present in the colloidal solution (Figure 1).

2.2. Elastic Imaging and Spectroscopy, Raman Measurements. The confocal imaging and spectroscopy of the elastically scattered light and of the Raman scattering were carried out using a Jobin-Yvon XploRa setup. After dilution, a few microliters of the colloidal solution were drop casted on a cleaned glass substrate. Figure 3 shows a typical bright field image recorded with the 50× objective. The bright points are the metallic nano-objects. Using a larger magnification it is possible to select one of these nano-objects. Indeed, with a 100× focusing objective (0.9 NA) our spatial resolution is diffraction limited to 355 nm (at 638 nm optical wavelength), which is the size of the small point in the dark field image (Figure 3). Since the nanoprism average size is around 150 nm, diffraction limited bright points could be due to an isolated

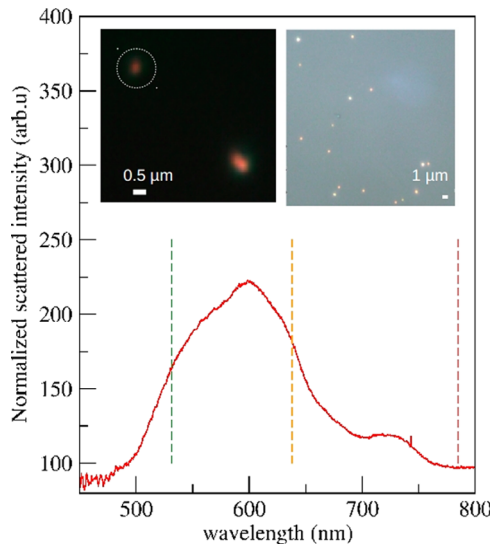


Figure 3. Elastic light scattering spectrum (Rayleigh) of a gold nano-object deposited on silica. The spectrum is obtained from the nano-object shown by a circle in the left dark field image (objective $\times 100$). The bright field on the top right shows a collection of dispersed nanoparticles (objective $\times 50$). The vertical dotted lines show the laser lines (532, 638, and 785 nm) used for the Raman experiment.

nanoisland but also to two or three aggregated nanoprisms. For instance, the brightest point in the dark field image (Figure 3) is certainly a larger aggregate. We avoided such objects and focused only on objects like those shown in the top left of the dark field image (i.e., diffraction limited and moderate brilliance). Its elastic scattering spectrum (recorded in the backscattering configuration) shows a surface plasmon resonance peaking around 600 nm (Figure 3). This resonance is blue-shifted with respect to the one measured from the colloidal solution because of the lower optical index of the surrounding medium. Indeed, the optical index of ethanol is around 1.36, which is larger than that of air/silica substrate (around 1.2). The surface plasmon resonance of the isolated nano-object (Figure 3) is narrower (around 150 nm fwhm) than the resonance recorded from the colloidal solution (Figure 2) because of the absence of inhomogeneous broadening effects.

Three laser lines 532, 638, and 785 nm were used to excite the Raman scattering. The laser beam was focused on the selected nano-object using the $100\times$ objective. In order to avoid possible degradation of the molecules surrounding the nano-object, due to laser heating, the incident intensity was limited to 1% of its maximum value (around 0.15 mW for 532 and 638 nm excitations and 0.8 mW for 785 nm excitation). The Raman spectra were recorded with a time step of 0.5 s and an accumulation time of 0.5 s.

3. RESULTS AND DISCUSSION

SERS experiments presented in this work involved a total of 13 isolated nano-objects such those shown in Figure 3. Repeating experiments on several nano-objects allows one to test the reproducibility of the results and to extract the main trends.

Figure 4 shows time-averaged Raman spectra of an isolated nano-object excited at 532, 638, and 785 nm. The spectra were normalized to the same accumulation time and laser power, in order to compare the relative intensities of the Raman scattering excited with the different excitation lines. As

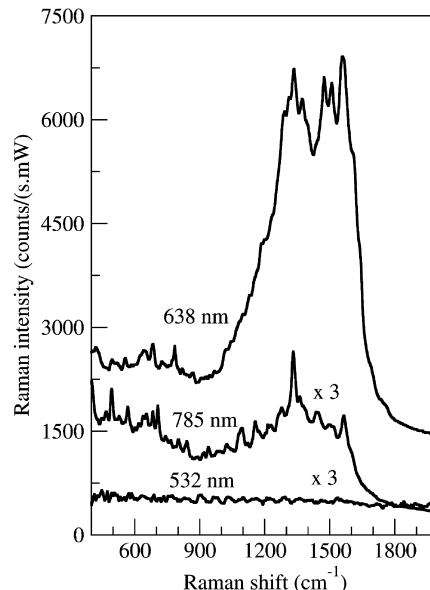


Figure 4. Raman spectra of an isolated gold nano-object. The spectra are averaged over an accumulation time of 2 min. The spectra excited at 532 and 785 nm have been magnified for clarity ($\times 3$). The intensity axis is in counts per second and per mW of incident laser power to allow for comparison of Raman intensities measured at the different excitation lines.

expected, the overall Raman intensity is maximum for excitation at 638 nm, i.e., close to the SPR of the isolated nano-object. This resonant behavior was consistently observed for all studied nano-objects, thus indicating the surface plasmon enhancement of the Raman scattering. The Raman features are due to the intramolecular vibrations of TREG and PVP molecules (to be discussed in detail further).

During the experiments, we have observed strong fluctuations of the Raman scattering intensities (Figure 5 and movie in Supporting Information). The snapshot spectra (Figure 5a,b) and the temporal SERS traces (Figure 5c,d) show that Raman features which are very weak or absent may become very intense (several thousand of counts/s), whereas other features may strongly fluctuate before disappearing. This phenomenon is well-known as SERS blinking^{38–41} and is typical of Raman scattering by a small number of molecules located at plasmonic hot spots.^{42,43} It is systematically observed in single molecule SERS experiments.^{44–46} The data presented in Figure 5a,b were acquired from two different isolated nano-objects. They are representative of the results obtained on the 13 nano-objects. In Figure 5a, mostly the Raman features of PVP are observed. While in Figure 5b, the Raman features of TREG are dominant. This assignment is based on density functional theory (DFT) calculations and on the comparison with reference Raman scattering spectra of TREG and PVP.

3.1. Assignment of the SERS Features. The assignment of the Raman features observed in the SERS measurements is not an easy task because of the sudden changes of the Raman signal. In addition, two molecular species, the PVP and the TREG, may contribute to the Raman scattering with similar spectral signatures. In order to identify the general trends, we have examined the experimental data obtained from the 13 studied nano-objects. Each nano-object is characterized by its temporal SERS trace. By carefully looking at all SERS traces, we

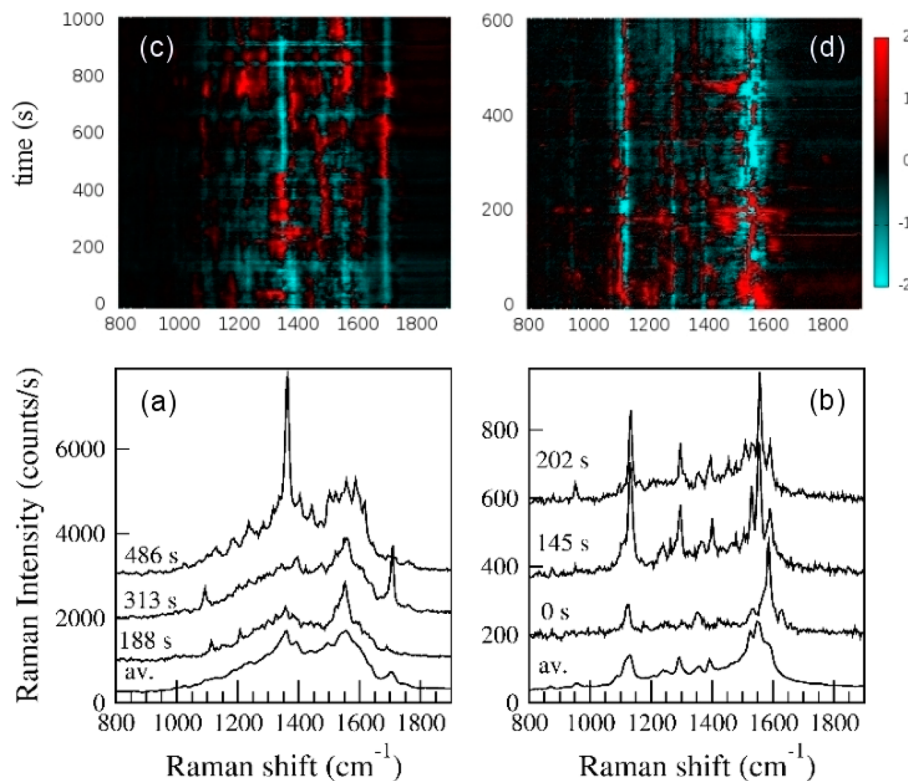


Figure 5. Snapshot SERS spectra of two isolated nano-objects (a and b). The excitation wavelength is 638 nm. The spectra averaged over the duration of the sequences are labeled “av”. The temporal traces of the Raman intensities are shown in (c) and (d). The latter were generated first by normalizing the Raman spectra to the same integrated intensity and then by calculating the difference between each normalized Raman spectrum and the (normalized) average spectrum.

were able to identify Raman features which are always present and exhibit strong intensity fluctuations.

On the basis of DFT calculations, and by comparison with the Raman spectrum of a PVP powder (see Supporting Information), we can unambiguously assign the peak around 1700 cm^{-1} (Figure 5a) to the stretching vibration mode of the $\text{C}=\text{O}$ bond in free PVP. Furthermore, the TREG has no Raman feature in this frequency range (Figure 5b). Remarkably, this peak is not always visible; for instance, at 188 and 486 s it is almost absent (Figure 5a), and this is the case most of the time (see Raman temporal trace in Figure 5c and movie in Supporting Information). We therefore suggest that the absence of the $\text{C}=\text{O}$ stretching peak around 1700 cm^{-1} indicates that the majority of the PVP molecules around the nanoparticle are not free but connected to the metal surface and thereby the CO stretching frequency is strongly shifted (i.e., no Raman signal around 1700 cm^{-1}). Molecules which are not bound to the nanoparticle surface are in a quasi-free state, and their $\text{C}=\text{O}$ stretching mode is around 1700 cm^{-1} . Therefore, in order to understand the SERS spectra and their temporal fluctuations, it is necessary to consider the vibration modes of a PVP molecule interacting with the metal surface. To do so, we have performed DFT calculations in which a single PVP molecule is bound to a single gold atom. Only one metal atom is considered in order to keep within a reasonable computation time, and we believe that this simple model is able to address the main effects of the molecule/nanoparticle surface interaction on the intramolecular vibrational properties. A similar approach has been reported by Mdluli et al.⁴⁷ for PVP-Au and PVP-Ag.

PVP could bind to gold via either the oxygen or the nitrogen atom. However, X-ray photoelectron spectroscopy (XPS) measurements^{48,49} showed that the binding of PVP to the surface of gold nanoparticles occurs via the oxygen atom in a donor–acceptor type interaction. In addition, our SERS measurements do not point to a strong involvement of the CN vibration modes. We therefore consider only the situation where a PVP molecule is connected to the gold atom via the oxygen atom. This corresponds to the complete or partial transfer of one electron from the $\text{C}=\text{O}$ double bond to the gold, thus forming a $\text{C}=\text{O}-\text{Au}$ complex.

In order to simulate different “interaction states” corresponding to different degrees of charge transfer between the molecule and the gold atom, we have changed the O–Au bond lengths. Indeed, in the DFT calculations, the O–Au distance can be fixed or left free. In the latter case, the O–Au distance is optimized (as the lengths of all other bonds) in order to minimize the total energy of the system. The Raman spectra calculated for various O–Au distances are shown in Figure 6. As can be seen, the frequency and intensity of the Raman features are very sensitive to the O–Au distance. These simulated spectra do not account for the plasmonic enhancement, since, in DFT, the calculation of the Raman scattering efficiency is based on the bond polarizability model.⁵⁰ However, they provide a good picture of the intensity and frequency fluctuations of the Raman peaks that may occur when the O–Au distance changes.

Let us first focus on the frequency range of the $\text{C}=\text{O}-\text{Au}$ modes. Figure 7 shows that the frequency of the $\text{C}=\text{O}-\text{Au}$ stretching mode increases linearly with increasing Au–O distance. In this mode, the Au atom is almost at rest because

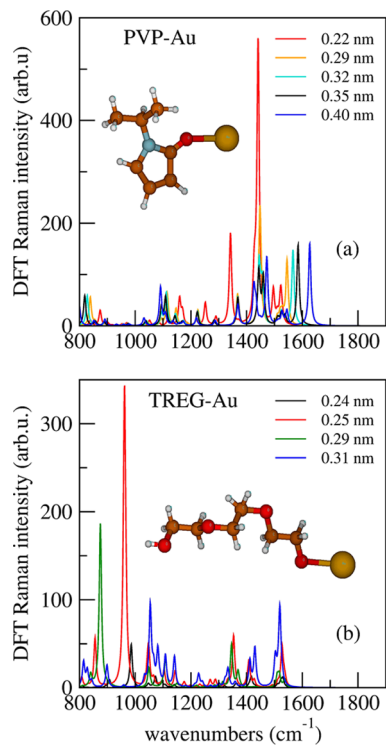


Figure 6. Raman spectra of PVP-Au (a) and TREG-Au (b) calculated using DFT for various O–Au bond lengths as indicated in the figures. The spectra were rescaled in order to fit the experimental vibrational frequencies (see Supporting Information).

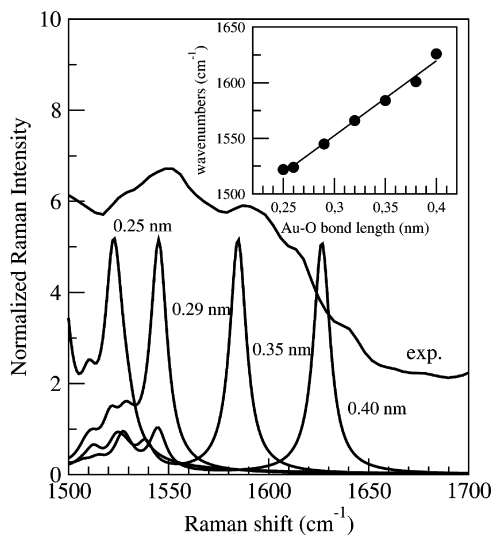


Figure 7. Average experimental Raman spectrum corresponding to Figure 5a and DFT Raman spectra calculated for different O–Au distances. The DFT spectra were normalized to the same maximum intensity. The inset shows the vibration frequency of the C–O–Au stretching mode as a function of the O–Au distance (in this mode the Au atom is at rest).

of its large mass. As expected, decreasing the O–Au distance increases the interaction strength of the oxygen atom with the heavy gold atom and hence slows down the mechanical motion. The comparison between the experimental time-averaged Raman spectrum and the DFT Raman spectra, in the frequency range of C–O–Au vibration modes, shows that the measured spectrum can be understood as the sum of the contributions of

C–O–Au vibration modes associated with different Au–O distances (Figure 7): in this frequency range, the Raman spectrum is inhomogeneously broadened by the fluctuations of the O–Au distance. This is corroborated by the fact that the bandwidth of the measured Raman spectrum is significantly larger than the line width of the Raman peaks observed in the snapshot spectra (Figure 5). So it appears that not only Raman intensity fluctuations take place, in the SERS blinking phenomenon investigated here, but also vibration frequency fluctuations. This has also been observed in single molecule SERS measurements.⁵¹ We thus assign both the Raman intensity and the vibration frequency fluctuations observed in our SERS experiments to “transient interaction states” between the molecules and the nanoparticle surface. The different O–Au distances used here in the DFT calculations allow for simulating the impact of these “transient interaction states” on the molecular vibrations.

In PVP, the oxygen atom is directly connected to the pyrrole ring. Hence, some of the vibration modes of the pyrrole ring may strongly involve the stretching of the CO bond. Indeed, the two intense peaks in the DFT Raman spectrum calculated for 0.22 nm O–Au distance (Figure 6) correspond to such modes. The 1350 cm⁻¹ mode is a totally symmetric breathing mode of the pyrrole ring involving a stretching of the C–O bond, whereas the 1450 cm⁻¹ mode is an asymmetrical deformation of the ring with a bending of the angle formed by the two carbons and the nitrogen atoms of the ring. This mode also involves a stretching of the C–O bond since one carbon is shared by the nitrogen and oxygen atoms. It is precisely around these two frequencies, 1350 and 1450 cm⁻¹, that we observe the main SERS peaks that exhibit significant intensity fluctuations (Figure 5a). It is interesting to notice that many other vibration modes of the pyrrole ring do not involve the CO bond stretching, and we did not observe remarkable Raman intensity fluctuations at these mode frequencies. With the CO bond being directly involved in the interaction with the gold surface, it is understandable that the corresponding vibration modes exhibit the strongest SERS features and the most important intensity fluctuations.

Let us now comment on the SERS acquired from another nano-object (Figure 5b,d). The Raman feature around 1100 cm⁻¹ is often observed and exhibits strong intensity fluctuations (see Supporting Information). It cannot be assigned to PVP because there are no vibration modes of C=O or C–O–Au bonds around this frequency in PVP. In fact, as mentioned above, the TREG acts not only as a solvent but also as a capping and stabilizing agent of the nanoparticles.³¹ It can therefore bind to the nanoparticle surface and give rise to SERS.

In order to investigate this situation, we considered a deprotonated TREG chain connected to the gold atom via the oxygen atom. The interaction is monitored by varying the O–Au distance. The DFT Raman spectra calculated for the different Au–O distance are presented in Figure 6. As for PVP-Au, one can notice the sensitivity of the Raman spectra to the Au–O interaction strength. The stretching vibration mode of the C–O–Au bond now falls in the 900–1200 cm⁻¹ range depending on the Au–O distance. Therefore, we assign the Raman features around 1100 cm⁻¹ (Figure 5b) to the stretching vibration mode of the C–O–Au. The wagging, rocking, and bending vibration modes of the CH groups contribute to the Raman scattering in the 1500–1600 cm⁻¹ frequency range.

It is worth mentioning that the number of TREG or PVP molecules may change from a nano-object to the other. In some objects we found mainly PVP SERS signature (Figure 5a), whereas in others the TREG SERS signal was clearly visible (Figure 5b). The assignment of the main Raman peaks is summarized in Table S1, Supporting Information.

3.2. Dynamics of the Molecule/Nanoparticle Interaction. Now that the main Raman features are identified, it is possible to investigate their temporal fluctuations and gain information on the dynamics of the interaction between the molecules and the nanoparticle surface.

First, for a given temporal sequence, we have normalized the Raman spectra to the same integrated intensity in order to get rid of the background fluctuations which will be discussed later. Then, we spectrally integrated the Raman intensities in the frequency range of the C=O and C—O—Au stretching modes of PVP and TREG and of the pyrrole ring breathing mode and plotted their time evolutions thus producing the Raman temporal traces presented in Figure 8.

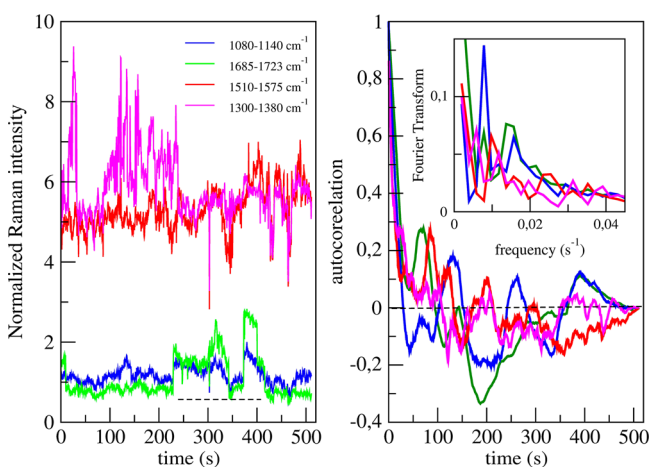


Figure 8. SERS temporal traces in the spectral ranges $1685\text{--}1723\text{ cm}^{-1}$ (C=O stretching in free PVP), $1510\text{--}1575\text{ cm}^{-1}$ (C—O—Au stretching in PVP-Au), $1300\text{--}1380\text{ cm}^{-1}$ (PVP pyrrole ring breathing in C—O—Au), and $1080\text{--}1140\text{ cm}^{-1}$ (C—O—Au stretching in TREG-Au). The horizontal dotted line indicates the range $230\text{--}420\text{ s}$ discussed in the text. Right panel shows the autocorrelation of the SERS temporal traces. The inset displays the Fourier transforms of the autocorrelation functions.

Consider the temporal trace associated with the stretching vibration mode of the C=O bond in free PVP ($1685\text{--}1723\text{ cm}^{-1}$). This signal is very weak at the beginning of the sequence which means that we do not observe free PVP molecules and that most of the molecules are bound to the nanoparticle surface. After 230 s, this signal becomes intense, a signature of the presence of free PVP molecules. It remains strong and fluctuating until 420 s. After that time, the signal becomes very weak, which we interpret as the return of the free PVP molecules to bound states with the nanoparticle surface.

The start (230 s) and finish (420 s) times of this sequence indicate that during 190 s free PVP molecules were present, thus giving rise to the C=O Raman feature around 1700 cm^{-1} . The rest of the time most of the PVP molecules are bound to the nanoparticle surface. Such a sequence can be repeated several times within a temporal SERS trace (see Supporting Information).

In order to characterize quantitatively the fluctuations of the SERS intensity, we have calculated the autocorrelation function of the SERS temporal traces signal (Figure 8).

The autocorrelation of the SERS signal associated with the C=O stretching vibrations of free PVP ($1685\text{--}1723\text{ cm}^{-1}$) is not an exponentially decreasing function of time as expected for random fluctuations; clear oscillations are observed. Indeed, the Fourier transform of the autocorrelation function (inset of Figure 8) reveals two Fourier components at 0.008 s^{-1} and 0.015 s^{-1} . The latter frequency could be the second harmonic of the fundamental frequency at 0.008 s^{-1} . These frequencies certainly reflect the complex physical–chemical phenomena underlying the dynamics of the molecule–nanoparticle surface interaction. Going deeper into the interpretation of the Fourier frequencies requires a detailed modeling of these phenomena. Nevertheless, we can conclude that the fluctuations of the SERS signal associated with the C=O stretching vibrations in free PVP are not random. A simple picture could be that if a group of PVP molecules is desorbed, it can readsorb back on the nanoparticle surface after a certain duration and that cycle can start again leading to quasi-periodic SERS intensity oscillations. Such desorption/readsoption cycles triggered by photo-induced metal-to-molecule charge transfer have already been invoked by Weiss and Haran.⁵²

We found a similar behavior for the SERS temporal trace in the range $1080\text{--}1140\text{ cm}^{-1}$ corresponding to the stretching vibration mode of C—O—Au bond in TREG-Au (Figure 8).

One can notice that in the $230\text{--}420\text{ s}$ interval (dotted lines in Figure 8), the SERS temporal traces associated with the CO stretching vibrations of free PVP and of TREG-Au are perfectly correlated (see movie in Supporting Information). This is corroborated by the autocorrelation function of TREG-Au which shows oscillations similar to those observed for the C=O stretching vibrations in free PVP. Its Fourier spectrum reveals the two same frequencies 0.008 and 0.015 s^{-1} . One possible explanation for this temporal correlation between the TREG-Au and free PVP SERS signals could be that if PVP molecules are desorbed from the nanoparticle surface they might be replaced by TREG molecules. This is an occasional exchange of TREG/PVP molecules which could be responsible for the correlated fluctuations of the TREG-Au and free-PVP SERS signals.

The SERS temporal trace in the $1510\text{--}1575\text{ cm}^{-1}$ range, associated with the stretching vibration modes of C—O—Au bond in PVP-Au, shows similar trends to those discussed above. Indeed, its autocorrelation function exhibits oscillations confirmed by the presence of a Fourier frequency at 0.01 s^{-1} . As discussed above, adsorption/desorption of PVP molecules and occasional TREG/PVP exchange events leave their fingerprint on the SERS signal fluctuations. Because of the molecular hindrance, such processes may cause conformational changes and rearrangements of the PVP molecules that kept connected to the nanoparticle surface, thus explaining the correlation between SERS intensity fluctuations associated with the C=O stretching vibrations in free PVP and in PVP-Au.

The SERS temporal trace in the $1300\text{--}1380\text{ cm}^{-1}$ range is associated with the breathing vibration mode of the PVP pyrrole ring. Unlike the other traces, its autocorrelation function shows a weak oscillatory behavior and seems to follow an exponential decay. This is corroborated by the absence of a clear nonzero Fourier frequency. Hence, at first sight, we might conclude that the intensity fluctuations of the SERS signal of the pyrrole breathing mode are random.

However, as will be shown now, some anticorrelation between the SERS signals of the pyrrole ring breathing and C=O stretching vibrations does exist.

To analyze quantitatively the cross-correlations between the SERS intensity fluctuations of the Raman lines, we have performed a 2D analysis of the temporal fluctuations. Following previous works,^{53,54} we have generated covariance maps using

$$\sigma(\nu_1, \nu_2) = \sum_{i=1}^N [I_i(\nu_1) - I_{av}(\nu_1)][I_i(\nu_2) - I_{av}(\nu_2)]$$

where N is the total number of acquired Raman spectra, and I_i and I_{av} are the i th and the average Raman spectra, respectively. The so-obtained covariance maps (Figure 9) show that the

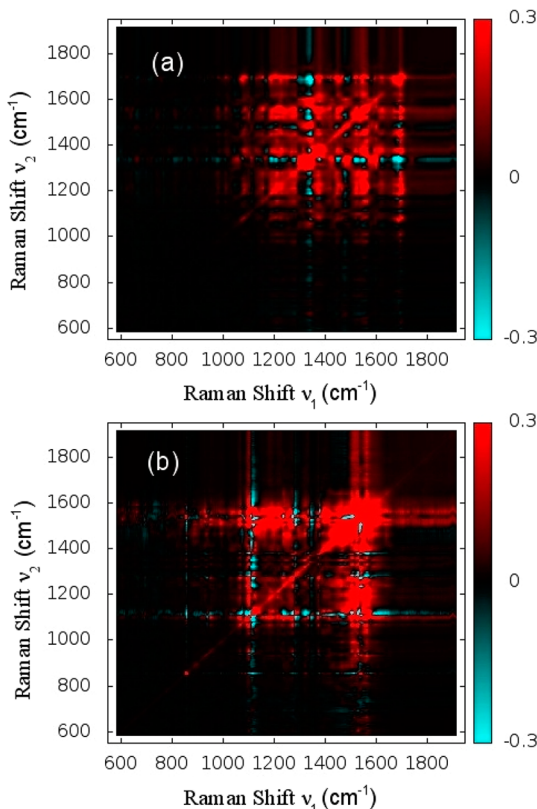


Figure 9. Covariance maps (a) and (b) of SERS intensity fluctuations generated from the data in Figure 5, panels a and b, respectively. Raman spectra were normalized to the same integrated intensity in order to get rid of the background fluctuations. Around 1000 spectra were used in the calculations.

temporal fluctuations of the SERS signal are not random; otherwise, the covariance values would be close to zero at all frequencies. Moreover, from the covariance map in Figure 9a (corresponding to Figure 5a), it is clear that the SERS signals of the C=O stretching mode in free PVP ($1685\text{--}1723\text{ cm}^{-1}$) and that of the C–O–Au stretching mode in TREG-Au ($1080\text{--}1140\text{ cm}^{-1}$) are strongly correlated, as already pointed out from the Fourier analysis of the temporal SERS traces (Figure 8). It is interesting to notice that the Raman line of TREG-Au around 1100 cm^{-1} is only weakly correlated with all other modes (of PVP-Au), which indicates that the adsorbed TREG and PVP molecules vibrate and fluctuate independently. Remarkably, the line around 1350 cm^{-1} associated with the totally symmetric (TS) breathing of the pyrrole ring is anticorrelated (i.e., shows

negative covariance values) with the nontotally symmetric (NTS) deformation of the pyrrole ring (1450 cm^{-1}) and especially with the C=O ($1685\text{--}1723\text{ cm}^{-1}$) and C–O–Au ($1510\text{--}1575\text{ cm}^{-1}$) stretching modes in free PVP and in PVP-Au, respectively.

By examining the time evolution of the SERS blinking reported for several molecules, Lombardi et al.⁵⁵ have pointed out that the SERS intensity (I_{TS}) from TS vibrations is governed by totally symmetric Franck–Condon (A) and vibronic coupling (C_{TS}) factors: $I_{TS} = (A + C_{TS})^2$, whereas the SERS intensity of NTS vibration involves only vibronic coupling (C_{NTS}): $I_{NTS} = C_{NTS}^2$. The Franck–Condon contribution is responsible for a constant Raman intensity, while the C_{TS} and C_{NTS} terms give rise to blinking. Because of the A term, the TS vibrations exhibit less blinking than the NTS. Moreover, as underlined by Lombardi et al.⁵⁵ destructive interference between A and C_{TS} terms may lower the TS SERS intensity. In our case, the C=O and C–O–Au stretching, which are NTS vibrations, exhibit the most drastic sudden changes in agreement with Lombardi et al.⁵⁵ arguments. On the other hand, since C_{TS} and C_{NTS} involve different vibronic coupling terms, no correlations between their SERS blinking is expected. This is certainly the reason why our 1350 cm^{-1} TS pyrrole breathing vibration shows no correlation with the NTS vibrations (1450 cm^{-1} pyrrole deformation, C=O and C–O–Au stretching). However, this argument does not explain the negative covariance values, i.e., the origin of the anticorrelations in Figure 9. A possible explanation has been proposed by Soontag et al.⁵⁶ These authors suggested that the fluctuations in orientation or surface adsorption geometry of the molecules may damp certain vibrational resonances while enhancing others thus leading to anticorrelated SERS signals. Here, we suggest that adsorption/readsoption of PVP molecules, which correspond to a breakdown of O–Au bonds and the formation of C=O bonds, may enhance the SERS signal of the NTS pyrrole deformation, C–O–Au and C=O stretching vibrations and correlative quench the TS breathing vibrations of the pyrrole ring thus leading to anticorrelated SERS blinking. As a matter of fact, from the temporal evolution of the Raman spectra one can easily notice that when the C=O stretching signal is strong, the signal of the pyrrole breathing mode is weak and vice versa (see movie in Supporting Information).

Figure 9b shows the covariance map corresponding to the Raman data in Figure 5b, where mainly the SERS features of TREG molecules are identified. The two covariance maps in Figure 9a,b are very different, which provides a mean of identifying the molecular species (PVP and TREG) giving rise to the Raman scattering. The main remarkable point in Figure 9b is the anticorrelation between the SERS signals of the C–O stretching mode (around 1100 cm^{-1}) and that of several modes in the range $800\text{--}1700\text{ cm}^{-1}$. As discussed above, this could be due to the damping of the C–O stretching mode by some molecular geometries and/or absorption/desorption events of TREG molecules. Such events are more difficult to detect in the case of TREG-Au, compared to PVP-Au, because of the overlapping between the vibration frequencies of TREG-Au and free TREG molecules.

It is worthwhile to mention that in single molecule SERS blinking is often analyzed in terms of the statistical distributions of the “bright” and “dark” time intervals which are described by inverse power laws.⁵⁷ The latter depend on energy barrier and duration of the optical trapping of the molecule in plasmonic hot spots. In our case we are not probing a single molecule but

a large ensemble of PVP and TREG molecules, and the SERS traces shown in Figure 8 cannot be interpreted in terms of random walk of molecules in and out of plasmonic hot spots; otherwise, the SERS fluctuations would not exhibit a quasi-periodic behavior as well as correlations or anticorrelations between the Raman lines associated with different molecules (PVP-Au, TREG-Au, and free PVP). Photoinduced adsorption/desorption events of PVP and TREG groups, assisted by strong local plasmonic fields, are more likely responsible for the SERS blinking observed in our experiments.

3.3. Role of the Optical Excitation. In order to address the role of the optical excitation in the dynamics of the molecule/nanoparticle surface interaction and in the SERS temporal fluctuations, we have measured the Raman spectra and their temporal fluctuations using the 785 nm excitation wavelength, which is tuned off the plasmonic resonance (Figure 3). The results are presented in Figure 10.

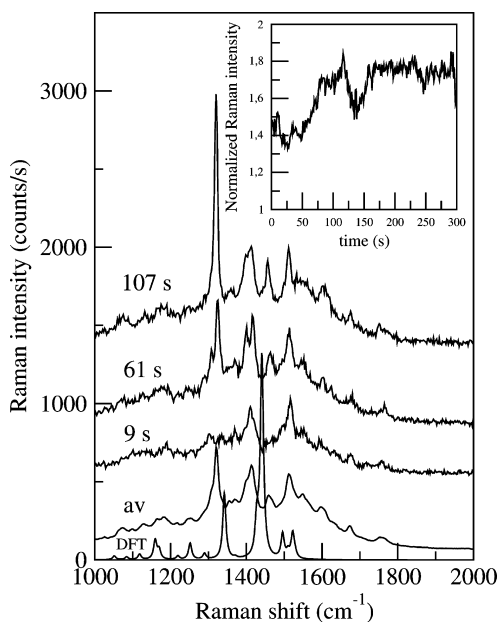


Figure 10. Snapshot Raman spectra excited with the 785 nm laser line. The time averaged spectrum is labeled “av”. The DFT Raman spectrum of PVP-Au calculated with 0.22 nm optimized O–Au distance is shown for comparison. The inset shows the temporal trace of the SERS signal integrated in the $1300\text{--}1600\text{ cm}^{-1}$ frequency range.

The Raman spectrum of the selected nano-object is dominated by the vibrational features of PVP-Au. The DFT Raman spectrum, calculated, for a PVP-Au molecule with an O–Au distance of 0.22 nm (i.e., optimum O–Au distance) is in good agreement with the time averaged spectrum. The snapshot spectra in Figure 10 correspond to the most important sudden changes. As indicated by the SERS temporal trace (inset of Figure 10), these fluctuations are however moderate compared to those observed (in Figure 5a) with 638 nm excitation (i.e., close to the LSPR). Over all the duration of the sequence (10 min), we did not observe the Raman feature corresponding to the C=O stretching mode in free PVP (around 1700 cm^{-1}), i.e., no desorption events of PVP molecules (see movie in Supporting Information). The observed SERS blinking is certainly due to thermally activated fluctuations of molecular orientation and conformation⁵² rather than to physical–chemical phenomena as those discussed

above. This suggests that the optical excitation plays an important role in the photoinduced chemical processes taking place at the nanoparticle surface.

3.4. Photochemistry at the Nanoparticle Surface.

Under resonant excitation of the surface plasmons, the absorption of laser photons is very effective. Nonlinear multiphotons absorption processes are also enhanced because of the large local electric field associated with the surface plasmons. Indeed, plasmonic enhancement of two-photon luminescence were reported in triangular gold nanoprisms.⁵⁸ Within a few tens of femtoseconds, the surface plasmons decay into electron–hole pair excitations of the metal nanoparticle and/or of the adsorbed molecules.⁵⁹ The photogenerated electrons and holes may in turn excite vibrations of the metal nanoparticle and of the adsorbed molecules.³⁷ They can also catalyze chemical reactions at the nanoparticle surface. On the basis of DFT calculations, Sun et al.⁶⁰ estimated the adsorption energy of a single oxygen atom on a gold surface between 2 and 3.5 eV, depending on the adsorption site, which is comparable to the energy stored by an electron–hole pair created by a single photon absorption (638 nm, corresponds to 1.94 eV). Hence, the absorption of one or two photons can break the Au–O bond leading to PVP or TREG molecule desorption. It is worthwhile to mention that the absorption spectrum of the adsorbed molecules combined with the large local field enhancement associated with surface plasmons may contribute to effective nonlinear optical absorption and generation of electron–hole pairs within the molecule itself. Indeed, from DDA simulations, we found that the enhancement of the plasmonic electric field at the nanoprism tips can reach a factor of 5. Hence, the absorption of two photons by molecules located at the plasmonic hot spots may reach a factor 600, since the absorption efficiency is proportional to the power 4 of the local electric field.⁵⁸ Moreover, the availability of molecular transitions at the multiphoton absorption energy can provide further enhancement of the nonlinear absorption process. In order to investigate this latter situation, we have calculated the optical absorption of a PVP-Au molecule using time-dependent DFT (TDFT) and including possible excitation of 20 unoccupied molecular orbitals (see Supporting Information).

As shown in Figure 11, the HOMO–LUMO transition is found at 1.29 eV. But a much stronger absorption is observed at higher energy around 5 eV. It is due to electronic transitions from the HOMO to high energy unoccupied molecular orbitals strongly hybridized with the gold atom orbitals. This calculation shows that high energy excited states are available for multiphoton absorption by the hybrid molecule/nanoparticle system. Due to plasmonic local field enhancement, such processes may be responsible for charge transfer and exchange between the molecule and the metal nanoparticle, thus leading to photocatalytic desorption of the molecules.

With laser excitation at 785 nm, we did not observe the signature of free PVP molecules (Figure 10). This is certainly due to the less effective optical absorption and generation of electron–hole pairs compared to 638 nm excitation. Nevertheless, after absorption of a 785 nm photon, the molecules may get into an excited state and relax the excess energy via orientational, conformational, and vibrational processes leading to random SERS blinking as observed in Figure 10.

It is worthwhile to mention that a signature of the presence of electron–hole pairs and their involvement in SERS is provided by the systematic observation of a broad background signal.⁶¹ Indeed, since the earlier work of Otto et al. it has been

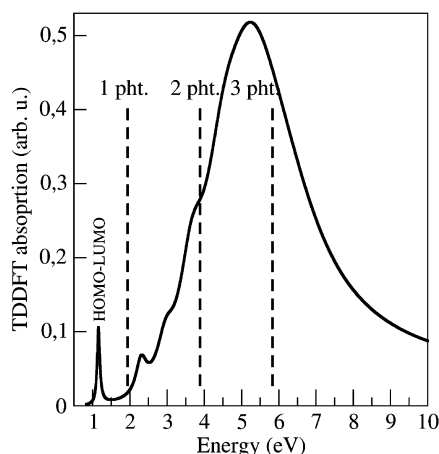


Figure 11. Optical absorption spectrum of a PVP molecule bound to a gold atom, calculated using TDDFT. The optimized O–Au distance is 0.22 nm. The sharp peak at 1.3 eV is due to the HOMO–LUMO transition, while the broad absorption band around 5.2 eV is due to transitions from the HOMO to the high energy unoccupied states. The dashed lines show the energy of one, two, and three 638 nm (1.94 eV) photon absorption processes.

recognized that the origin of this Raman scattering background is connected with the photogeneration of electron–hole pairs⁶¹ within the metal nanoparticle. More recently, it has been shown^{53,54} that the intensity fluctuations of the background signal are correlated with the SERS signal fluctuations. Since the presence of the background signal is the signature of the photogenerated electron–hole pairs, it is interesting to perform a 2D analysis of the SERS fluctuations including the background contribution.

Figure 12 shows the correlation map, corresponding to the Raman data of Figure 5a with background included (i.e.,

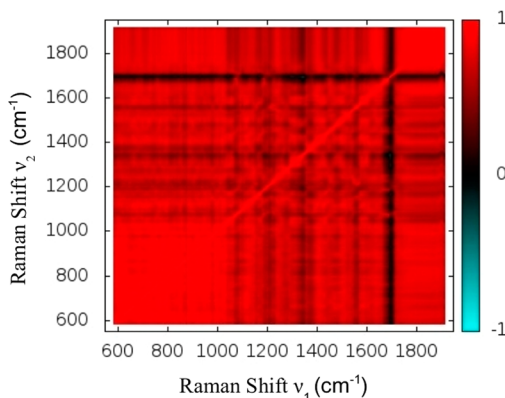


Figure 12. Correlation map generated with the Raman data corresponding to Figure 5a including the background contribution. Correlation, rather than covariance, is more useful because of the large scale variations in covariance values when the background contribution is included.

without intensity normalization). As can be seen, strong positive correlation values are obtained at frequencies where there is no Raman line because the background is very broad (see movie in Supporting Information). Remarkably, at the frequencies of the Raman lines associated with the molecular vibrations, there is only weak correlations between the SERS intensities and the background intensity. This is particularly

marked for the 1700 cm⁻¹ line associated with the C=O stretching mode of free PVP. This indicates that the SERS intensity of the molecular vibrations and the background intensity fluctuate almost independently. That is why we suggest that the excitation of optical transitions within the adsorbed molecules, by plasmonic enhanced single and multiphoton absorption, is responsible for the release of molecules from the nanoparticle surface rather than photocatalytic reactions induced by the electron–hole pairs photo-generated within the metal nanoparticle.

4. CONCLUSION

We have synthesized gold nanoprisms using a simple one-pot chemical process. These nanoprisms exhibit a strong plasmonic resonance which is exploited to produce SERS from the stabilizing molecules. Owing to a diffraction-limited laser beam focus, we observed the blinking of the SERS signal from isolated nano-objects. Using vibrational dynamics calculations, based on density functional theory, we were able to identify and assign the Raman active vibrations directly involved in the molecule/nanoparticle interaction. We could then produce SERS temporal traces, in the relevant spectral ranges, which we analyzed quantitatively using the autocorrelation function and its Fourier transform. In that way, we showed that, under resonant excitation of the surface plasmons, the SERS fluctuations are not random and exhibit a quasi-periodic behavior. Our interpretation for this experimental finding is that molecules bound to the nanoparticle surface undergo desorption/adsorption events in quasi-periodic sequences. We also generated covariance maps of the SERS fluctuations and thus pointed out cross-correlations between the SERS signals at different frequencies. We found clear correlations between the vibration modes of TREG and PVP molecules which we assigned to dynamical exchange events of PVP/TREG molecules. Finally, we suggested that photoinduced surface chemical reaction mechanisms can explain the observed fluctuations of the SERS signals. This interpretation is supported by time-dependent DFT calculations of the molecular optical absorption. The reported results shed light on the complex interaction between the stabilizing molecules and the metal nanoparticle surface. They also contribute to a better understanding of the SERS blinking phenomenon which is still a matter of numerous investigations and debates.

ASSOCIATED CONTENT

Supporting Information

(i) Assignment of the Raman features, (ii) density functional theory calculations, and (iii) four video clips showing the temporal fluctuations of the signal excited at 638 and 785 nm. This material is available free of charge via the Internet at <http://pubs.acs.org>.

AUTHOR INFORMATION

Corresponding Author

*E-mail: adnen.mlayah@cemes.fr. Tel: +33 05 62 25 78 36.

Notes

The authors declare no competing financial interest.

ACKNOWLEDGMENTS

A.M. gratefully acknowledges support by the Ministry of Higher Education and Scientific Research of Tunisia. This work was

supported by the CALMIP high performance computing facilities at Paul Sabatier University of Toulouse.

■ REFERENCES

- (1) Kelly, K. L.; Coronado, E.; Zhao, L. L.; Schatz, G. C. The Optical Properties of Metal Nanoparticles: The Influence of Size, Shape, and Dielectric Environment. *J. Phys. Chem. B* **2003**, *107*, 668–677.
- (2) Lee, K. S.; El-Sayed, M. A. Gold and Silver Nanoparticles in Sensing and Imaging: Sensitivity of Plasmon Response to Size, Shape, and Metal Composition. *J. Phys. Chem. B* **2006**, *110*, 19220–19225.
- (3) Munehika, K.; Smith, J. M.; Chen, Y.; Ginger, D. S. Plasmon Line Widths of Single Silver Nanoprism as a Function of Particle Size and Plasmon Peak Position. *J. Phys. Chem. C* **2007**, *111*, 18906–18911.
- (4) Ringe, E.; McMahon, J. M.; Sohn, K.; Cobley, C. M.; Xia, Y.; Huang, J.; Schatz, G. C.; Marks, L. D.; Van Duyne, R. P. Unraveling the Effects of Size, Composition, and Substrate on the Localized Surface Plasmon Resonance Frequencies of Gold and Silver Nanocubes: A Systematic Single-Particle Approach. *J. Phys. Chem. C* **2010**, *114*, 12511–12516.
- (5) Daniel, M. C.; Astruc, D. Gold Nanoparticles: Assembly, Supramolecular Chemistry, Quantum-Size-Related Properties, and Applications Toward Biology, Catalysis, and Nanotechnology. *Chem. Rev.* **2004**, *104*, 293–346.
- (6) Rosi, N. L.; Mirkin, C. A. Nanostructures in Biodiagnostics. *Chem. Rev.* **2005**, *105*, 1547–1562.
- (7) Corma, A.; Garcia, H. Supported Gold Nanoparticles as Catalysts for Organic Reactions. *Chem. Soc. Rev.* **2008**, *37*, 2096–2126.
- (8) Mayer, K. M.; Hafner, J. H. Localized Surface Plasmon Resonance Sensors. *Chem. Rev.* **2011**, *111*, 3828–3857.
- (9) Biju, V. Chemical Modifications and Bioconjugate Reactions of Nanomaterials for Sensing, Imaging, Drug Delivery and Therapy. *Chem. Soc. Rev.* **2014**, *43*, 744–764.
- (10) Dreaden, E.; Alkilany, A.; Huang, X.; Murphy, C.; El-Sayed, M. The Golden Age: Gold Nanoparticles for Biomedicine. *Chem. Soc. Rev.* **2012**, *41*, 2740–2779.
- (11) Chen, G.; Qiu, H.; Prasad, P. N.; Chen, X. Upconversion Nanoparticles: Design, Nanochemistry, and Applications in Theranostics. *Chem. Rev.* **2014**, *114*, 5161–5214.
- (12) Fievet, F.; Lagier, J. P.; Blin, B. Homogeneous and Heterogeneous Nucleations in the Polyol Process for the Preparation of Micron and Submicron Size Metal Particles. *Solid State Ionics* **1989**, *32/33*, 198–205.
- (13) Jeanmaire, D. L.; Van Duyne, R. P. Surface Raman Spectroelectrochemistry: Part I. Heterocyclic, Aromatic, and Aliphatic Amines Adsorbed on the Anodized Silver Electrode. *J. Electroanal. Chem. Inter. Electrochem.* **1977**, *84*, 1–20.
- (14) Sharma, B.; Frontiera, R. R.; Henry, A. I.; Ringe, E.; Van Duyne, R. P. SERS: Materials, Applications, and the Future. *Mater. Today* **2012**, *15*, 16–25.
- (15) Kneipp, K.; Moskovits, M.; Kneipp, H. *Surface-Enhanced Raman Scattering*; Springer: Heidelberg, 2006.
- (16) Eric, R. L.; Pablo, E. *Principles of Surface Enhanced Raman Spectroscopy and Related Plasmonic Effects*; Elsevier: Amsterdam, 2009.
- (17) Sonntag, M. D.; Klingsporn, J. M.; Zrimsek, A. B.; Sharma, B.; Ruvuna, L. K.; Van Duyne, R. P. Molecular Plasmonics for Nanoscale Spectroscopy. *Chem. Soc. Rev.* **2014**, *43*, 1230–1247.
- (18) Nie, S.; Emory, S. R. Probing Single Molecules and Single Nanoparticles by Surface-Enhanced Raman Scattering. *Science* **1997**, *275*, 1102–1106.
- (19) Schmid, T.; Opilik, L.; Blum, C.; Zenobi, R. Nanoscale Chemical Imaging Using Tip-enhanced Raman Spectroscopy: A Critical Review. *Angew. Chem., Int. Ed.* **2013**, *52*, 5940–5954.
- (20) Alyssa, B.; Zrimsek; Henry, A. I.; Van Duyne, R. P. Single Molecule Surface-Enhanced Raman Spectroscopy Without Nanogaps. *J. Phys. Chem. Lett.* **2013**, *4*, 3206–3210.
- (21) Le Ru, E. C.; Etchegoin, P. G. Quantifying SERS Enhancements. *Mater. Res. Bull.* **2013**, *38*, 631–640.
- (22) Anker, J. N.; Hall, W. P.; Lyandres, O.; Shah, N. C.; Zhao, J.; Van Duyne, R. P. Biosensing with Plasmonic Nanosensors. *Nat. Mater.* **2008**, *7*, 442–453.
- (23) Cao, Y. C.; Jin, R.; Mirkin, C. A. Nanoparticles with Raman Spectroscopic Fingerprints for DNA and RNA Detection. *Science* **2002**, *297*, 1536–1540.
- (24) Qian, X.; Peng, X. H.; Ansari, D. O.; Yin-Goen, Q.; Chen, G. Z.; Shin, D. M.; Yang, L.; Young, A. N.; Wang, M. D.; Nie, S. M. In Vivo Tumor Targeting and Spectroscopic Detection with Surface-Enhanced Raman Nanoparticle Tags. *Nat. Biotechnol.* **2008**, *26*, 83–90.
- (25) Kneipp, K.; Wang, Y.; Kneipp, H.; Perelman, L. T.; Itzkan, I.; Dasari, R. R.; Feld, M. S. Single Molecule Detection Using Surface-Enhanced Raman Scattering (SERS). *Phys. Rev. Lett.* **1997**, *78*, 1667–1670.
- (26) Klingsporn, J. M.; Jiang, N.; Pozzi, E. A.; Sonntag, M. D.; Chulhai, D.; Seideman, T.; Jensen, L.; Hersam, M. C.; Van Duyne, R. P. Intramolecular Insight into Adsorbate-Substrate Interactions via Low Temperature, Ultrahigh Vacuum Tip-Enhanced Raman Spectroscopy. *J. Am. Chem. Soc.* **2014**, *136*, 3881–3887.
- (27) Valley, N.; Greenelch, N.; Van Duyne, R. P.; Schatz, G. C. A Look at the Origin and Magnitude of the Chemical Contribution to the Enhancement Mechanism of Surface-Enhanced Raman Spectroscopy (SERS): Theory and Experiment. *J. Phys. Chem. Lett.* **2013**, *4*, 2599–2604.
- (28) Yamamoto, Y. S.; Ishikawa, M.; Ozaki, Y.; Itoh, T. Fundamental Studies on Enhancement and Blinking Mechanism of Surface-enhanced Raman Scattering (SERS) and Basic Applications of SERS Biological Sensing. *Front. Phys.* **2014**, *9*, 31–46.
- (29) Xiong, Y.; Washio, I.; Chen, J.; Cai, H.; Li, Z.; Xia, Y. Poly(vinyl pyrrolidone): A Dual Functional Reductant and Stabilizer for the Facile Synthesis of Noble Metal Nanoplates in Aqueous Solutions. *Langmuir* **2006**, *22*, 8563–8570.
- (30) Xia, X.; Zeng, J.; Oetjen, L.; Li, Q.; Xia, Y. Quantitative Analysis of the Role Played by Poly(vinylpyrrolidone) in Seed-Mediated Growth of Ag Nanocrystals. *J. Am. Chem. Soc.* **2012**, *134*, 1793–1801.
- (31) Mezni, A.; Balti, I.; Mlayah, A.; Jouini, N.; Smiri, L. S. Hybrid Au-Fe₃O₄ Nanoparticles: Plasmonic, SERS and Phase Transition Properties. *J. Phys. Chem. C* **2013**, *177*, 16166–16174.
- (32) Seth, M.; Silverstein, W.; Jensen, L. Theoretical Studies of Plasmonics Using Electronic Structure Methods. *Chem. Rev.* **2011**, *111*, 3962–3994.
- (33) Millstone, E.; Sarah Hurst, J.; Gabriella Métraux, S.; Joshua Cutler, I.; Chad Mirkin, A. Colloidal Gold and Silver Triangular Nanoprism. *Small* **2009**, *5*, 646–664.
- (34) Draine, B. T.; Flatau, P. J. The Discrete Dipole Approximation for Periodic Targets: I. Theory and Tests. *J. Opt. Soc. Am. A* **1994**, *11*, 1491–1499.
- (35) Draine, B. T.; Flatau, P. J. *User Guide to the Discrete Dipole Approximation Code DDSCAT 7.2*, 2012, <http://arXiv.org/abs/1202.3424>.
- (36) Blaber, M. G.; Henry, A. I.; Bingham, J. M.; Schatz, G. C.; Van Duyne, R. P. LSPR Imaging of Silver Triangular Nanoprism: Correlating Scattering with Structure Using Electrodynamics for Plasmon Lifetime Analysis. *J. Phys. Chem. C* **2012**, *116*, 393–403.
- (37) Marty, R.; Baffou, G.; Arbouet, A.; Girard, C.; Quidant, R. Charge Distribution Induced Inside Complex Plasmonic Nanoparticles. *Opt. Express* **2010**, *18*, 3035–3044.
- (38) Maruyama, Y.; Ishikawa, M.; Futamata, M. Thermal Activation of Blinking in SERS Signal. *J. Phys. Chem. B* **2004**, *108*, 673–678.
- (39) Agapov, L. R.; Malkovskiy, V. A.; Sokolov, P. A.; Foster, D. M. Prolonged Blinking with TERS Probes. *J. Phys. Chem. C* **2011**, *115*, 8900–8905.
- (40) Domke, K. F.; Zhang, D.; Pettinger, B. Enhanced Raman Spectroscopy: Single Molecules or Carbon. *J. Phys. Chem. C* **2007**, *111*, 8611–8616.
- (41) Neacsu, C. C.; Dreyer, J.; Behr, N.; Raschke, M. B. Scanning-probe Raman Spectroscopy with Single-molecule Sensitivity. *Phys. Rev. B* **2006**, *73*, 193406–193409.

- (42) Maruyama, Y.; Ishikawa, M.; Futamata, M. Re-examining the Origins of Spectral Blinking in Single-molecule and Single-nanoparticle SERS. *J. Phys. Chem. B* **2004**, *108*, 13119–13127.
- (43) Emory, R. S.; Jensen, A. R.; Wenda, T.; Han, M.; Nie, S. Re-examining the Origins of Spectral Blinking in Single-molecule and Single-nanoparticle SERS. *Faraday Discuss.* **2006**, *132*, 249–259.
- (44) Zhang, W.; Yeo, B. S.; Schmid, T.; Zenobi, R. Single Molecule Tip-Enhanced Raman Spectroscopy with Silver Tips. *J. Phys. Chem. C* **2007**, *111*, 1733–1738.
- (45) Ichimura, T.; Watanabe, H.; Morita, Y.; Verma, P.; Kawata, S.; Inouye, Y. Temporal Fluctuation of Tip-Enhanced Raman Spectra of Adenine Molecules. *J. Phys. Chem. C* **2007**, *111*, 9460–9464.
- (46) Sonntag, M.; Klingsporn, J.; Garibay, L.; Roberts, J.; Dieringer, J.; Scheidt, K.; Jensen, L.; Schatz, G. C.; Seideman, T.; Van Duyne, R. P. Single-Molecule Tip-Enhanced Raman Spectroscopy. *J. Phys. Chem. C* **2012**, *116*, 478–483.
- (47) Mdluli, M.; Ndabenhle, S. N.; Revaprasadu, P.; Karamanis, J.; Leszczynski. Surface Enhanced Raman Spectroscopy (SERS) and Density Functional Theory (DFT) Study for Understanding the Regioselective Adsorption of Pyrrolidinone on the Surface of Silver and Gold Colloids. *J. Mol. Struct.* **2009**, *935*, 32–38.
- (48) Huang, H. H.; Ni, X. P.; Loy, G. L.; Chew, C. H.; Tan, K. L.; Loh, F. C.; Deng, J. F.; Xu, G. Q. Photochemical Formation of Silver Nanoparticles in Poly(*N*-vinylpyrrolidone). *Langmuir* **1996**, *12*, 909–912.
- (49) Jiang, P.; Zhou, J. J.; Li, R.; Gao, Y.; Sun, T. L. PVP-capped Twinned Gold Plates from Nanometer to Micrometer. *J. Nanopart. Res.* **2006**, *8*, 927–934.
- (50) Tomasi, J.; Mennucci, B.; Cammi, R. Quantum Mechanical Continuum Solvation Models. *Chem. Rev.* **2005**, *105*, 2999–3094.
- (51) Le Ru Eric, C.; Pablo, G. E. Single-Molecule Surface-Enhanced Raman Spectroscopy. *Annu. Rev. Phys. Chem.* **2012**, *63*, 65–87.
- (52) Weiss, A.; Haran, G. Time-Dependent Single-Molecule Raman Scattering as a Probe of Surface Dynamics. *J. Phys. Chem. B* **2001**, *105*, 12348–12354.
- (53) Amy, A. M.; Michele, L. J.; Nadia, B.; Kathy, L. R.; David, M. J. 2D Correlation Analysis of the Continuum in Single Molecule Surface Enhanced Raman Spectroscopy. *J. Am. Chem. Soc.* **2005**, *127*, 7292–7293.
- (54) Bizzarri, A. R.; Cannistraro, S. Statistical Analysis of Intensity Fluctuations in Single Molecule SERS Spectra. *Phys. Chem. Chem. Phys.* **2007**, *9*, 5315–5319.
- (55) Lombardi, J. R.; Birke, R. L.; Haran, G. Single Molecule SERS Spectral Blinking and Vibronic Coupling. *J. Phys. Chem. C* **2011**, *115*, 4540–4545.
- (56) Sonntag, M. D.; Chulhai, D.; Seideman, T.; Jensen, L.; Van Duyne, R. P. The Origin of Relative Intensity Fluctuations in Single-Molecule Tip-Enhanced Raman Spectroscopy. *J. Am. Chem. Soc.* **2013**, *135*, 17187–17192.
- (57) Kitahama, Y.; Tanaka, Y.; Itoh, T.; Ozaki, Y. Power-law Statistics in Blinking SERS of Thiacyanine Adsorbed on a Single Silver Nanoaggregate. *Phys. Chem. Chem. Phys.* **2010**, *12*, 7457–7460.
- (58) Viarbitskaya, S.; Teulle, A.; Marty, R.; Sharma, J.; Girard, C.; Arbouet, A.; Dujardin, E. Tailoring and Imaging the Plasmonic Local Density of States in Crystalline Nanoprisms. *Nat. Mater.* **2013**, *12*, 426–432.
- (59) Moores, A.; Goettmann, F. The Plasmon Band in Noble Metal Nanoparticles: An Introduction to Theory and Applications. *New J. Chem.* **2006**, *30*, 1121–1132.
- (60) Sun, K.; Kohyama, M.; Tanaka, S.; Takeda, S. Theoretical Study of Atomic Oxygen on Gold Surface by Hückel Theory and DFT Calculations. *J. Phys. Chem. A* **2012**, *116*, 9568–9573.
- (61) Otto, A. Surface Enhanced Raman Scattering of Adsorbates. *J. Raman Spectrosc.* **1991**, *22*, 743–752.